# Efficient On-board Signaling Processing for Satellite-Terrestrial Integrated Core Networks

Yu Liu, Luhan Wang, Ao Liu, Zhaoming Lu, Guochu Shou, Adlen Ksentini

***Abstract*—Integrating Low-Earth Orbit (LEO) satellite constellations with terrestrial mobile networks can achieve global coverage and complement terrestrial networks. The inherent mobility of satellites induces frequent handovers of User Equipment (UE), generating massive signaling. Coupled with limited satellite resources, the Network Functions (NFs) deployed on satellites cannot process these signaling promptly, leading to increased queuing time. Additionally, the movement of on-board NFs increases the distance to UE, extending propagation delay. Extended Procedure Completion Time (PCT) of control plane procedures degrades user plane Quality of Service (QoS). To address the above challenges, we propose a satellite-terrestrial integrated core network architecture to enhance signaling processing performance. Firstly, we redesign the control plane network functions and introduce a Satellite-Ground Synergy Method (SGSM), categorizing signaling into time-sensitive and time-tolerant types. The former is processed on-board, while the latter is handled terrestrially, utilizing a designed UE context synchronization mechanism. Furthermore, migration is employed to counteract the movement. We devise a migration procedure to reduce transferred data during migration. Moreover, we model instance migration as a Markov Decision Process and proposed an online NFs migration algorithm based on deep reinforcement learning to determine migration timing and target satellites. Extensive experiments demonstrate that the proposed methods significantly reduce queuing time and the volume of transferred data, while also exhibiting superior performance in terms of propagation delay and the frequency of migrations.**

***Index Terms*—LEO networks, core network, signaling processing, satellite-terrestrial integrated networks, dynamic migration, signaling classification.**

## I. Introduction

It is estimated that approximately 4 billion people worldwide still lack Internet access [1]. Extending connectivity to these underserved regions is crucial for the progression of future mobile networks [2]. Low Earth Orbit (LEO) satellites offer a cost-effective solution for global coverage. Due to their closer proximity to Earth compared to Geostationary Earth Orbit (GEO) and Medium Earth Orbit (MEO) satellites, LEO satellites provide higher bandwidth, lower transmission losses, and shorter communication delay [3]. Starlink has launched LEO satellites equipped with Direct to Cell technology, enabling them to deliver standard Long-Term Evolution (LTE) services to unmodified terrestrial cell phones. They plan to commence text services this year, followed by voice, data, and Internet of Things (IoT) services in 2025 [4]. The integration of satellite and terrestrial networks to provide ubiquitous services is a critical component in achieving the goals of 6th Generation mobile networks.

Several specifications for the integration of satellite and 5th Generation mobile networks (5G) have been outlined by the 3rd Generation Partnership Project (3GPP) [5]. Deploying next-generation NodeBs (gNBs) on satellites provides an economical approach to expand the service coverage of terrestrial mobile networks [6]. Notably, when the core network (CN) is located on the ground, satellite networks transparently relay control plane signaling and user plane data to the ground, significantly extending the Procedure Completion Time (PCT) of control plane [7]–[9]. Regardless of the type of service, the establishment, modification, and deletion of the user plane require management by the control plane. Prolonged control plane procedures will decrease user plane Quality of Service (QoS) [8]. For instance, while a prolonged handover procedure may have little impact on short message services, it can significantly degrade real-time communication services such as voice and video calls, as well as video streaming and online gaming, leading to lag or even interruptions.

Leveraging satellite computing resources facilitates on-board Network Functions (NFs) to process signaling expeditiously without forwarding it to the ground. Wang *et al.* [10] proposed that deploying NFs directly onto satellites endows the satellite networks with fundamental core functions, thereby enhancing network management and reducing latency. The advantages of on-board NFs were highlighted in [9]. Xing *et al.* [11] demonstrated the feasibility of on-board NFs, successfully completing registration and session establishment procedures. J. Kim *et al.* [8] utilized satellites as both core and access networks, redesigning the session establishment and handover procedures to decrease the PCT of User Equipment (UE) accessing via satellite. In [12], multiple NFs were deployed on a single satellite. Additionally, deploying User Plane Function (UPF) on satellites can establish a 5G Local Area Network [13], enabling direct data forwarding without detouring to the ground. In our previous work [14], we explored the integration of UPF with a LEO constellation, designed the operational mode of the satellite UPF (S-UPF), and proposed algorithms to determine the optimal deployment location of the

Yu Liu, Luhan Wang, Zhaoming Lu, and Guochu Shou are with the School of Information and Communication Engineering, the Beijing Laboratory of Advanced Information Networks, and the Beijing Key Laboratory of Network System Architecture and Convergence, Beijing University of Posts and Telecommunications, Beijing 100876, China (E-mail: {buptliuyu, wluhan, lzy0372, gcshou}@bupt.edu.cn). Corresponding author: Luhan Wang.

Ao Liu is with the School of Information and Communication Engineering, Beijing University of Posts and Telecommunications, and also with the Key Laboratory of Universal Wireless Communications, Ministry of Education, Beijing 100876, China (E-mail: ao.liu@bupt.edu.cn).

Adlen Ksentini is a professor in the Communication Systems Department of EURECOM in Sophia Antipolis, France, e-mail: adlen.ksentini@eurecom.fr.

This work was supported in part by the National Key Research and Development Program of China under Grant 2024YFE0200300 and in part by the Beijing Natural Science Foundation (L222003).

S-UPF. By processing and forwarding data directly in space, the transmission time of data and the PCT are significantly reduced.

Although transmission to the ground is avoided, limited resources and satellite mobility increase queuing and forwarding hops, thereby extending the PCT and impairing user plane QoS. The two primary factors affecting PCT are the queuing time within the NF and the signaling propagation time. Firstly, the rapid movement of satellites leads to frequent handovers of UE between satellite gNBs (S-gNBs) [7], [8], [15], resulting in plentiful signaling between gNBs and the CN. Scarce satellite resources, such as storage, computing, and power, limit the horizontal or vertical scalability of NFs within satellites. Failure to process signaling promptly increases queuing time. Furthermore, as emphasized by the author in [16], if the service remains on the satellite (i.e., the NF drifts with the satellite), the number of hops between the UE and the service increases, leading to higher propagation delay. This also raises the risk of control procedure failures due to unreliable Inter-Satellite Links (ISLs) in outer space, thereby increasing the possibility of service interruptions or network inaccessibility.

Ensuring efficient on-board signaling processing performance entails two primary challenges: 1) enhancing on-board processing capabilities to maintain acceptable queuing time under high signaling loads, and 2) mitigating increased propagation time caused by NF mobility. To address the first challenge, previous works [17]–[20] have proposed offloading requests to other satellites to accelerate mission completion when local resources are insufficient. However, these strategies are not suitable for signaling processing. Since signaling processing depends on the UE context, satellite mobility incurs significant overhead in maintaining the latest UE context across multiple satellites. Migration is a viable approach to address the second challenge, and there is extensive researches on the migration of on-board services [7], [21]–[23]. However, migration algorithms for control plane NFs that simultaneously consider the distribution of UE and S-UPFs have yet to be explored. Considering these two factors is essential because user plane management requires interaction among control plane NFs, gNBs/UE, and UPFs.

To address the aforementioned challenges, we propose a satellite-terrestrial integrated core network architecture aimed at enhancing signaling processing performance through two primary objectives: reducing signaling processing time and propagation time. To tackle the first challenge, we have redesigned the control plane network functions, introducing the Reorganization Control Plane Function (RCPF) and deploying it on satellites. To the best of our knowledge, we are the first to propose the Satellite-Ground Synergy Method (SGSM), which leverages terrestrial resources to facilitate on-board processing. In SGSM, signaling is categorized into two types: time-sensitive signaling is processed on-board, while time-tolerant signaling is processed on the ground. To achieve collaborative signaling processing, we designed a pioneering UE context synchronization mechanism between the RCPF and the terrestrial core network (TCN). To address the second challenge through migration, we designed a migration procedure for the RCPF to reduce the amount of transferred data during migration. Additionally, to further optimize the migration strategy, we model the RCPF migration problem into a Markov Decision Process (MDP). We then proposed an innovative Real-time On-board Control Plane Migration (ROCPM) algorithm, considering the distribution of UE and S-UPFs based on deep reinforcement learning, to determine the optimal migration timing and the target satellite.

The major contributions of this work are as follows:

- We propose a satellite-terrestrial integrated core network architecture, wherein signaling is categorized into time-sensitive and time-tolerant types. The former is processed on-board, while the latter is handled terrestrially, based on a UE context synchronization mechanism.
- We design a migration procedure for the RCPF to decrease the transferred data during migration. Additionally, we develop a migration algorithm to optimize migration timing and the target satellite, considering the distribution of UE and S-UPFs.
- We conduct extensive experiments to evaluate the performance of the proposed architecture, procedure, and algorithm. The experimental results demonstrate that our methods significantly reduce queuing time and the volume of transferred data , while also showing superior performance in terms of propagation time and the number of migrations.

The remainder of the paper is organized as follows: Section II reviews related work. Section III introduces our proposed satellite-terrestrial integrated core network architecture. Section V details the migration procedure, model, and algorithm. Section VI presents and analyzes the results of the experiment. Finally, Section VII concludes the paper and suggests future research directions.

## II. RELATED WORK

**Signaling Processing in Terrestrial Mobile Core Networks:** Service-Based Architecture (SBA) facilitates NF instance collaboration, but inter-NF message exchanges introduce significant protocol overhead [24]. In [25], multiple NFs were deployed on a single machine with shared memory for inter-NF interaction, thereby reducing time spent on serialization, deserialization, and signaling transmission. To streamline signaling processing procedures, [26] designed new NFs tailored to specific procedures, consolidating the services of all NFs involved in signaling processing into a single NF to eliminate the additional overhead of inter-NF interactions. Similarly, in [27], the authors proposed purpose-oriented functional re-composition to decrease redundant information management across multiple NFs. In [28], a unified stateless instance handles all signaling, relying on a database for coordination.

Adopting the stateless approach decouples NF processing from its context [7], allowing any instance with the latest context to provide services immediately. In [29], each NF instance retrieved up-to-date UE context from the database and synchronized modified user context back to the database, enabling dynamic instance scaling. However, statelessness is not suitable for LEO constellations due to the substantial overhead introduced by frequent interactions between instances

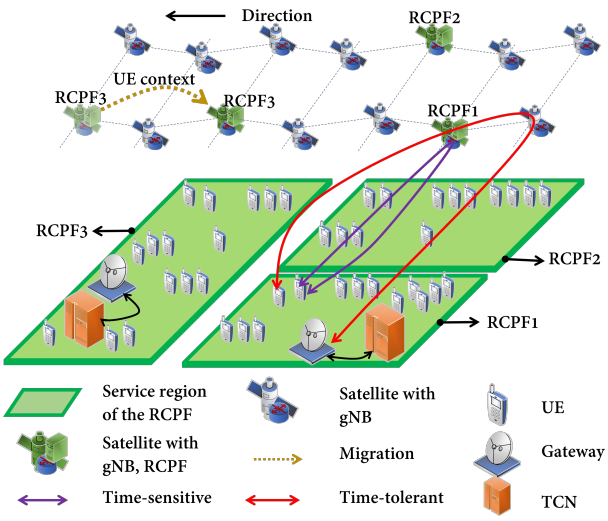


Fig. 1. The green box indicates the region allocated for each RCPF. The red line delineates the processing pathway for time-tolerant signaling, while the purple line signifies the processing pathway for time-sensitive signaling.

and databases. Regardless of whether the database is located on the satellite or the ground, it incurs high access costs for one party. Furthermore, the reliability of interactions is reduced by laser-based wireless ISLs in outer space.

**Satellite Computation:** Deploying services on satellites to provide on-board computing is poised to become an essential paradigm for the future [20]. The integration of multiple satellites can enhance service processing capacity. In scenarios with insufficient local resources, Han *et al.* in [17] proposed that satellites utilize resources from others to improve service provision. The authors in [18] assigned tasks to other LEO satellites via ISLs for achieving load balancing. Similarly, in [19], the authors jointly optimized service request dispatching and service placement. However, leveraging multiple satellites to augment signaling processing is inefficient for signaling processing. The NF must synchronize the latest UE context with neighboring and numerous non-adjacent satellites. Maintaining up-to-date UE context across different satellites increases system complexity and overhead within the satellite system, thereby reducing link utilization rates in space.

Dynamic service deployment is an effective strategy in LEO constellations. Han *et al.* [21] proposed service migration based on the variations in upstream and downstream traffic. Sun *et al.* [30] highlighted the importance of deploying NFs on appropriate satellites, considering the spatial and temporal dynamics of service demands and active user numbers. The authors in [22] introduced a dynamic Software-Defined Networking (SDN)-enabled satellite network where the SDN controller was periodically reconfigured to minimize average flow setup time. In [31], optimal K edge servers were activated at different time, with each satellite assigned to the appropriate server, adapting to the dynamic LEO network.

**Satellite-Terrestrial Integrated Mobile Network:** Some research has been dedicated to integrating satellite and terrestrial networks. To address large-scale UE access, the authors in [6] proposed cooperative batch mechanisms to compress signaling transmission and reduce power consumption. In [8], satellites served as both the core and access network, with session establishment and handover procedures redesigned to minimize PCT. The authors in [12] redesigned procedures for UE and S-gNB, enhancing the flexibility of mobility management for UE and S-gNBs by deploying multiple NFs on the satellite. However, deploying multiple NFs on a single satellite will rapidly deplete resources. Our previous work [7] implemented a distributed deployment strategy for the Access and Mobility Management Function (AMF), Session Management Function (SMF), and UPF within the satellite domain, determining the optimal distribution of NF instances. In [14], we developed an algorithm to statically allocate ground areas to S-UPF instances. By leveraging prior knowledge of the ephemeris, we transformed the S-UPF deployment problem over a future period into the shortest path problem in a graph. In [32], Li *et al.* decoupled states from orbital NFs and utilized state management with device-as-the-repository. Authentication and User Security Functions and UPF were deployed on each satellite, while some control procedures are still to be forwarded to the TCN.

Many studies utilize on-board resources for processing, but they overlook signaling processing under high-load conditions. Additionally, they do not account for the distinct characteristics of various signaling types, nor do they consider the deployment of the control plane about the distribution of S-UPFs and UE.

## III. Satellite-Terrestrial Integrated Core Network Architecture

### A. Reorganized Control Plane Function

Deploying NFs on satellites to process signaling promptly, without transmitting them to the ground, is illustrated in Fig. 1. In the SBA architecture [33], each NF has specific functionalities and provides distinct services. This necessitates the coordination of multiple NFs to process signaling. For instance, registration and session establishment procedures involve approximately 6 to 7 NFs [26]. The distributed deployment of these NFs across satellites [7] introduces additional latency and overhead due to the interactions between on-board NFs.

Deploying multiple NFs on a single satellite can mitigate the issues of inter-satellite interactions among different on-board NFs. However, using Hypertext Transfer Protocol (HTTP) for communication between NFs introduces significant time and resource overheads due to the serialization and deserialization processes. To reduce PCT and enhance signaling processing efficiency, we reorganized control plane NFs. Given that a single signaling process often involves multiple services across different NFs, various code segments from multiple NFs need to collaborate. We extract these code segments and integrate them into the RCPF, which is deployed on the satellite. The RCPF avoids interactions between NFs on different satellites and eliminates the communication overhead among NFs within the satellite. For instance, during a handover, services such as $NF_{amf}^{HO}$ and $NF_{smf}^{HO}$ are utilized, where $NF_{amf}^{HO}$ denotes

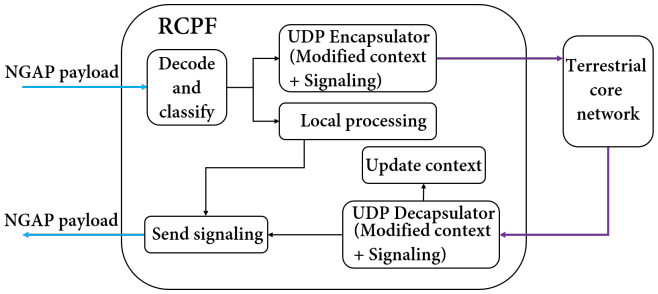


Fig. 2. Cooperation between RCPF and TCN.

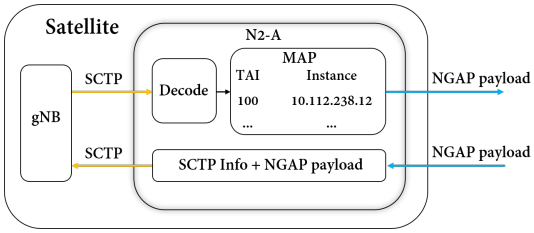


Fig. 3. N2 Interface Agent

the service within the AMF responsible for handling the handover signaling. By aggregating these services, we form $RCPF = \{NF^{HO}_{amf}, NF^{HO}_{smf}\}$. This integration allows signaling processing to be handled entirely within the RCPF, obviating the need for coordination between the AMF and SMF.

### B. Satellite-Ground Synergy Method

The dynamic coverage region caused by the movement of the on-board RCPF, combined with uneven terrestrial traffic, leads to congestion and longer signaling processing time within the RCPF. In particular, when certain signaling processes require extensive processing time, it can cause other signaling time out. Notably, the PCT of different procedures impacts the UE experience in varying degrees. Indiscriminate processing of various types of signaling can result in timeouts for some procedures. For example, a 200 ms increase in PCT might be acceptable for registration, deregistration, and Protocol Data Unit (PDU) session release procedures. However, such delay is unacceptable for the handover, as its completion time significantly affects user plane performance. This delay can lead to timeouts in TCP-based data traffic, thereby reducing application throughput [25].

Fig. 2 illustrates the SGSM. Given the varying PCT requirements across different procedures, we classify these procedures into time-sensitive and time-tolerant categories, and design a UE context synchronization mechanism accordingly. When the signaling reaches the RCPF, it is decoded to ascertain the message type and determine the necessity of on-board processing. If so, the RCPF processes it using the local context and sends a response, as depicted by the purple line in Fig. 1. Otherwise, the RCPF forwards the signaling to the TCN, along with any modified context, as represented by the red line in Fig. 1. Upon receiving the signaling, the TCN updates its local UE context with the enclosed context and processes the signaling. Subsequently, the TCN attaches the updated context to the signaling and returns it to the RCPF. The RCPF then utilizes the attached UE context to update its own context and forwards the signaling to the UE. Due to the sequential characteristic of the signaling process, rather than parallel, the RCPF and TCN will not alter the context simultaneously, thereby ensuring the consistency of the UE context.

Moreover, the gNB transmits signaling to the CN, and the CN may or may not send a response. In scenarios where the gNB sends signaling without requiring a response from the CN (e.g., *PDU Session Resource Setup Response*), the RCPF must process such signaling. Otherwise, forwarding these signaling to the TCN would result in UE context inconsistencies between the TCN and RCPF. This inconsistency arises because, even if the TCN promptly returns the updated context to the RCPF, new signaling might arrive at the RCPF during this interval. The outdated on-board local context prevents the RCPF from correct processing.

### C. Migration and Static Assignment

To maintain the proximity of the RCPF to the UE effectively, our approach partitions the Earth's surface into zones, with some zones forming a region, as illustrated in Fig. 1. Each region is serviced by a designated RCPF instance. The size of the RCPF service area is adjusted based on traffic density and the RCPF's capacity.

Satellite movement increases the distance between the UE and corresponding RCPF instance, migration is applied to avoid increased signaling transmissions. Instance migration modifies the connectivity between the gNB and the CN and disrupts Next Generation Application Protocol (NGAP) connections based on the connection-oriented Stream Control Transmission Protocol (SCTP). To maintain standard procedures without altering the gNB's operational logic, we propose the N2 interface Agent (N2-A), co-located with each gNB on the same satellite, as depicted in Fig. 3. The N2 interface is utilized for control plane signaling between the AMF and the gNB. Each N2-A establishes an SCTP connection with its on-board gNB and extracts and forwards NGAP messages to the RCPF.

Each region has a dedicated RCPF instance, so the N2-A must identify the appropriate satellite. We design a region-to-instance map within the N2-A. The target instance IP address will be transmitted to the N2-A after migration. When the N2-A needs to transmit the NGAP payload to the RCPF, it utilizes the UE location information within the NGAP payload to determine the UE's regional affiliation and then forwards the signaling to the correct satellite by querying the map. Since the movements of satellites are predictable, their positions can be obtained in advance. Consequently, the region-to-instance map will be transmitted to the new satellite upon entering a new region.

## IV. Migration Model and Placement Algorithm

Despite the processing capability of a single RCPF has been enhanced in section III, the PCT continues to escalate

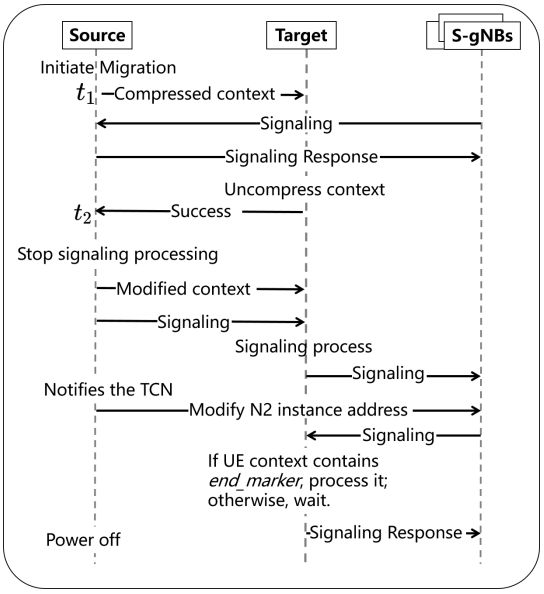


Fig. 4. Migration procedure for RCPF

as the RCPF drifts with the satellite. The migration of RCPF instances raises three critical questions: 1) How should the RCPF be migrated? 2) To which satellite should the RCPF migrate? 3) When should the migration occur? To address these issues, we propose a migration procedure, model, and algorithm.

### A. Migration Procedure

Unlike traditional virtual machine (VM) or container migrations, which involve transferring the operational state, NF instance migration focuses on context transfer. To avoid disrupting signaling processing, it is necessary to ensure that the latest context is utilized during signaling processing and that the context remains consistent after migration.

One method is that the target instance requests each UE context from the source instance upon receiving new signaling. However, the target instance may retrieve incorrect UE context. For instance, consider a scenario where the UE transmits two sequential signaling, and the S-gNB modifies the N2 interface address after sending the first signaling. The first and second signaling are sent to the source and target instances, respectively. Upon receiving signaling, the target instance fetches the UE context from the source instance. However, if the source instance has not yet processed the first signaling, it leads to incorrect signaling processing at the target instance. Furthermore, the target instance needs to initiate a UE context retrieval for each UE, resulting in increased signaling processing time and a substantial amount of duplicate data. For example, the Public Land Mobile Network (PLMN) information for each UE may be identical, yet it will be redundantly transferred multiple times due to the presence of multiple UE.

To reduce the amount of transferred data and to avoid each UE experiencing context acquisition delay, we propose a migration procedure as illustrated in Fig. 4. At time $t_1$, the migration decision is made. The source instance compresses all context and transmits them to the target instance. The consistent format of the context and repetitive fields enhance compression efficiency. The source instance still handles signaling until it receives confirmation from the target instance at time $t_2$, indicating successful reception of the compressed context.

At time $t_2$, the source instance ceases processing signaling and forwards all incoming signaling to the target instance. If the UE context is modified between $t_1$ and $t_2$, the source instance sends these updates, along with the *end_marker*, to the target instance. The *end_marker* signifies the latest UE context. If the source instance currently uses the UE context for processing, it stops the processing and sends the signaling, any modified context, and the *end_marker* to the target instance. The source instance then notifies the TCN to update its address to that of the target instance and instructs the N2-A to update the N2 interface address. Upon the signaling arriving at the target instance, the signaling is immediately processed if the UE context contains the *end_marker*; otherwise, the processing is delayed until the *end_marker* is received.

### B. System Model

We consider the set of satellites denoted as $\mathcal{S} = \{s_1, s_2, \ldots, s_V\}$. Each satellite establishes ISLs with neighboring satellites within the same and adjacent orbits, adhering to a well-established "grid" topology [34]. For satellites in the first and last orbits, their opposite travel directions result in significant relative velocity, preventing the formation of ISLs. The rapid movement of satellites leads to a continuously dynamic network topology. We define the set of time slots as $\mathcal{T} = \{1, 2, 3, \ldots, T\}$. Within each time slot, we assume that inter-satellite delay and satellite resources are constant. The delay between the $i$-th and $j$-th satellites at time $t$, denoted as $d^t(i, j)$, is computed using the Dijkstra algorithm [35].

The distance and elevation angle between UE and each satellite continually change, influencing the quality of communication. At each time slot, the UE selects a satellite for access based on criteria such as the longest connectivity duration, lowest satellite load, or nearest proximity. In this study, we assume each UE connects to the nearest satellite.

The ground is divided into zones $\mathcal{A} = \{a_1, a_2, a_3, \ldots, a_A\}$, where each zone $a_i$ has a population denoted as $a_i^L$. It is assumed that the UE can directly establish connections with the S-gNB [36]. The connectivity between terrestrial zone $a_i$ and satellite $s_j$ at time $t$ is represented by $\alpha_{i,j}^t$, where $\alpha_{i,j}^t = 1$ indicates a connection, and $\alpha_{i,j}^t = 0$ indicates no connection. Thus, the load on each satellite can be represented as follows:

$$l_{s_j}^t = \sum_{i=1}^{A} a_i^L * \alpha_{i,j}^t \tag{1}$$

As user plane traffic exceeds control plane traffic, more S-UPFs need to be deployed. Assuming there are $M$ S-UPFs within the RCPF's service region, it is essential to deploy the S-UPF and RCPF on separate satellites to ensure timely data forwarding. Due to the satellite movements, both the RCPF and S-UPF may drift away from the UE or exit their

designated regions, necessitating continuous migration. The placement of S-UPFs directly influences user plane QoS. Thus, the migration of S-UPF is prioritized at the start of each time slot. It is assumed that UE selects the S-UPF with minimal delay. The variable $y_{i,j}^t = 1$ indicates that the $i$-th S-UPF is allocated to the $j$-th satellite at time $t$, while $y_{i,j}^t = 0$ indicates its absence. The connectivity between terrestrial zones and S-UPFs is denoted by $\beta_{i,k}^t$, where $\beta_{i,k}^t = 1$ signifies that zone $a_i$ is served by the $k$-th S-UPF at time slot $t$, and $\beta_{i,k}^t = 0$ otherwise. In 5G networks, with the separation of the control and user planes, any user plane management necessitates interactions between the control plane, UPF, and gNB/UE. Satellite movements and S-UPF migrations result in variations in communication time between the RCPF, S-gNB/UE, and S-UPF. Following the completion of S-UPF migration (whether the S-UPF migrates to another satellite depends on the migration strategy), the RCPF determines whether and where to migrate based on its current position, UE distribution, and the locations of the S-UPFs.

This study primarily focuses on the time-sensitive Xn-based handover procedures due to the unchanging RCPF and the presence of ISLs. The Xn interface, which connects gNBs, facilitates signaling and data forwarding. Xn-based handover refers to the UE handover between gNBs via the Xn interface. Multiple RCPFs are deployed to ensure global service, with each RCPF assigned to specific terrestrial zones, a subset of $\mathcal{A}$. Each RCPF must remain within its designated service region. For clarity, this paper focuses on a single RCPF service region, as the methodology can be similarly applied to other RCPF regions. The location of the RCPF is represented by $\mathcal{X}$:

$$\mathbf{X} = \begin{bmatrix} x_1^1 & x_1^2 & \cdots & x_1^T \\ x_2^1 & x_2^2 & \cdots & x_2^T \\ \vdots & \vdots & \ddots & \vdots \\ x_V^1 & x_V^2 & \cdots & x_V^T \end{bmatrix}$$

where $x_i^t = 1$ indicates the presence of the RCPF on satellite $s_i$ at time $t$, and $x_i^t = 0$ indicates its absence. The assignment of each zone to the RCPF is denoted by $\gamma_i$, where $\gamma_i = 1$ means that $a_i$ is served by the RCPF, and $\gamma_i = 0$ means that $a_i$ is served by another RCPF.

*1) Procedure Completion Time:* The Xn-based handover procedure is depicted in Figure 5. The UE disconnects from the current S-gNB before P0 and establishes a connection with the new S-gNB at P0. During P1 and P2, the target S-gNB address is transmitted to the S-UPF, and during P3 and P4, the S-UPF address is forwarded to the target S-gNB. The PCT represents the time required to transfer the bearer from the source S-gNB to the target S-gNB, including the propagation time of P1, P2, P3, and P4, as well as the processing time of the RCPF and S-UPF. At time $t$, the transmission time of the Xn-based handover in zone $a_i$ is calculated as:

$$\begin{aligned} D_{i,t}^{'} =& 2d^t(\sum_{j=1}^{V} \alpha_{i,j}^t s_j, \sum_{j=1}^{V} x_j^t s_j) \\ &+ 2d^t(\sum_{j=1}^{V}\sum_{k=1}^{M} \beta_{i,k}^t y_{k,j}^t s_j, \sum_{j=1}^{V} x_j^t s_j) \end{aligned} \tag{2}$$

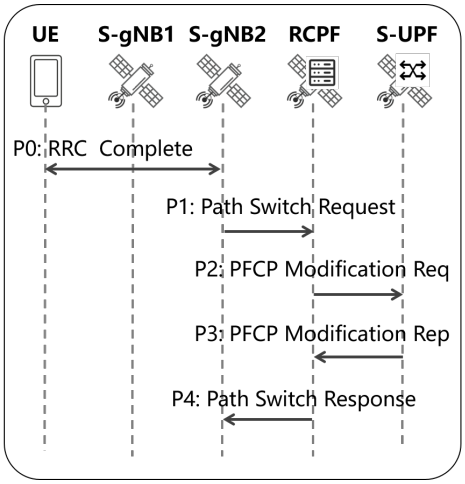


Fig. 5. Xn-based handover procedure.

Given the non-simultaneous launch of satellites, their hardware exhibits differences. The computing capacity of the $j$-th satellite, denoted as $U_{s_j}$, is measured in CPU cycles per second. We assume that the computing capacity of each satellite follows a normal distribution, $U_{s_j} \sim \mathcal{N}(\mu, \sigma^2)$. As the number of UE connected to a satellite increases, additional resources are required to maintain S-gNB performance. Assuming a linear relationship between the computing resource utilized by the gNB and its load [37], the remaining computing resources available for onboard NFs are expressed as:

$$U_{s_j}^{'} = U_{s_j} - (\varphi * l_{s_j}^t) \tag{3}$$

where $\varphi$ is a proportionality coefficient that depends on the gNB performance.

The total CPU cycles required by the RCPF for Xn-based handover signaling is $q_c$, and for S-UPF is $q_u$. Thus, at time $t$, the PCT for the Xn-based handover in zone $a_i$ is given by:

$$D_{i,t}^* = 2\frac{q_c}{U_{\sum_{j=1}^{V} x_j^t s_j}^{'}} + \frac{q_u}{U_{\sum_{j=1}^{V}\sum_{k=1}^{M} \beta_{i,k}^t y_{k,j}^t s_j}^{'}} \tag{4}$$

Hence, the average PCT in the RCPF service region at time $t$ is:

$$D_t^{ave} = \frac{1}{\sum_{j=1}^{A} \gamma_j a_j^L} \sum_{i=1}^{A} \gamma_i (D_{i,t}^{'} + D_{i,t}^*) a_i^L \tag{5}$$

*2) Migration Model:* While migration reduces the distance between the NF instance and the UE, it incurs additional operational costs. Intermediate satellites between the source and target satellite must forward substantial volumes of UE context, consuming bandwidth and energy. Furthermore, migration can increase PCT, and the inherent unreliability of space may lead to migration failures. Thus, migrations should be performed judiciously and infrequently.

We use the number of migrations to measure the cost. Given the service deployment decisions $x^{t-1}$ at time $t-1$ and $x^t$ at time $t$, the total number of migration times over a period $T$

is:

$$Mt = \sum_{t=1}^{T-1} F(\sum_{j=1}^{V} x_j^t s_j, \sum_{j=1}^{V} x_j^{t+1} s_j) \tag{6}$$

where $F(s_i, s_j)$ is used to denote the migration of RCPF.

$$F(s_i, s_j) = \begin{cases} 0, & s_i = s_j \\ 1, & s_i \neq s_j \end{cases} \tag{7}$$

*3) Problem Formulation:* The objectives of RCPF deployment are twofold: 1) minimizing the PCT, and 2) reducing the number of migrations. However, these objectives are contradictory. Minimizing PCT necessitates more frequent migrations, and the optimal outcome depends on the relative weights assigned to each objective. Therefore, the optimization goal can be formulated as:

$$\mathcal{P}1 : \min_{\mathbf{X}} \frac{1}{T}(\sum_{t=1}^{T} w_1 D_t^{ave} + w_2 Mt) \tag{8}$$

$$s.t. \begin{cases} C1 & : \sum\limits_{i=1}^{V} x_i^t = 1, \forall t \in [1, T] \\ C2 & : \sum\limits_{j=1}^{V} \alpha_{i,j}^t = 1, \forall i \in [1, A] \\ C3 & : \sum\limits_{i=1}^{V} y_i^t + x_i^t \leq 1, \forall t \in [1, T] \\ C4 & : \sum\limits_{k=1}^{M} \beta_{i,k}^t = 1, \forall i \in [1, A] \end{cases} \tag{9}$$

where $w_1$ and $w_2$ are weight factors. Constraint C1 ensures that the RCPF is deployed on only one satellite at any given time. Constraint C2 guarantees that each zone can connect to only one satellite at a time. Constraint C3 ensures that the RCPF and S-UPF are not simultaneously deployed on the same satellite. Constraint C4 ensures that each zone connects only one S-UPF.

### *C. Real-time On-board Control Plane Migration*

For Problem 10, it is essential to determine, at each time slot, whether migration should be initiated and identify the optimal migration destination. Additionally, the current decision will impact subsequent decisions. The RCPF migration in dynamic satellite networks is formulated as a 0-1 Nonlinear Programming problem, which can be reformulated as a Dynamic Uncapacitated Facility Location Problem (DUFLP). Here, the RCPF, serving all UE within its assigned region, is analogized as a facility. Over time, the load on each satellite varies, similar to evolving client demands. The RCPF migration procedure is conceptualized similarly to factory relocation. Since the Dynamic Uncapacitated Facility Location Problem is NP-hard [38], the RCPF migration problem in satellite networks is also NP-hard.

We propose the ROCPM algorithm, leveraging Deep Reinforcement Learning (DRL) to address the migration problem, where the RCPF acts as an intelligent agent. Reinforcement learning is a machine learning approach that enables agents to learn by interacting with environment and receiving rewards, aiming to maximize cumulative rewards. DRL is a subset of reinforcement learning methods that employ neural networks to replace traditional state-action tables. Unlike supervised learning, which relies on labeled input-output pairs, DRL seeks to balance the exploration of various actions and their outcomes with the exploitation of current knowledge to maximize cumulative rewards. We formalize the RCPF placement problem as an MDP, a decision-making model that mathematically characterizes an environment through Actions, States, and Rewards.

States: At time $t$, the state space of an agent includes the previous deployment decision of the RCPF, inter-satellite delay, S-UPF locations, and the available computing resources of the satellites.

Actions: The action denotes the target location for RCPF migration at the current time. If the target location coincides with the current location, it implies no migration.

$$r(t) = -r_1 D_t^{ave} - \begin{cases} 0, & t = 1 \\ r_2 F(\sum_{j=1}^{V} x_j^{t-1} s_j, \sum_{j=1}^{V} x_j^t s_j), & t > 1 \end{cases} \tag{10}$$

Reward: Upon making a deployment decision, the agent immediately receives a reward. The reward function is integral to the MDP and should be designed to align with the initial optimization objective outlined in 10. The reward consists of two components. The first component is the delay. The second component imposes a penalty on the number of migrations to discourage frequent migrations. The coefficients $r_1$ and $r_2$ are used to weigh these components.

State Transition: The state transition function reflects the dynamic nature of the satellite network. In the considered scenario, we assume that the state transition function is unknown to the agent. The dynamics of the environment encompass changes in the agent's position, S-UPF locations, inter-satellite delay, and variations in the available computing resources of satellites.

The ROCPM algorithm, denoted as Algorithm 1, initializes the replay memory $D$ with a specified capacity and initializes both the action-value function $Q$ and the target action-value function $Q'$ with random weights $\omega$. The algorithm iterates over a maximum number of episodes, initializing the environment at the beginning of each episode. At each time step within an episode, the algorithm retrieves the available action space $A(s_t)$, where $s_t$ is the current state. It then employs an $\epsilon$-greedy strategy to select an action. With probability $\epsilon$, it randomly selects an available action from $A(s_t)$; otherwise, it selects the action that maximizes the action-value function $Q(s_t, a; \omega)$ within the available action space. The $\epsilon$-greedy strategy serves as an exploration mechanism for agents in the environment, addressing the issue of agents getting stuck in local optima and premature convergence. An $\epsilon$-exponential decay strategy is employed to explore the environment extensively in the early stages of training. After executing the selected action, the algorithm stores the tuple $(s_t, a_t, r_t, s_{t+1})$ in the replay memory $D$. Periodically, a random batch of experience is sampled from $D$ to update the action-value

**Algorithm 1:** Real-time On-board Control Plane Migration Algorithm

Initialize replay memory $D$
Initialize action-value function $Q$ with random weights $\omega$
Initialize target action-value function $Q'$ with weights $\omega' = \omega$
**for** episode = 1 to MaxEpisode **do**
  Initialize state $s_1$
  **for** t = 1 to T **do**
    Get the available action space $A(s_t)$
    Randomly select an available action $a_t \in A(s_t)$ with probability $\epsilon$
    Otherwise, select $a_t = \arg\max_{a \in A(s_t)} Q(s_t, a; \omega)$
    Execute action $a_t$ in the environment and observe reward $r_t$ and next state $s_{t+1}$
    Store transition $(s_t, a_t, r_t, s_{t+1})$ in replay memory $D$
    Sample a random batch of experiences $(s_j, a_j, r_j, s_{j+1})$ from $D$
    Set $y_j =$
    $$\begin{cases} r_j & \text{if } s_{j+1} \text{ is terminal} \\ r_j + \gamma \max_{a'} Q(s_{j+1}, a'; \omega') & \text{otherwise} \end{cases}$$
    Perform a gradient descent step on $(y_j - Q(s_j, a_j; \omega))^2$ with respect to the network parameters $\omega$
    Every $C$ episodes, update target network: $\omega' = \omega$
  **end for**
**end for**

function $Q$. For the migration of RCPF, the current migration action impacts future states. When updating the action-value function, the algorithm computes the target $y_j$ by considering future rewards with the discount factor $\gamma$. A gradient descent step is then performed on the mean squared error between the predicted Q-value and the target. Additionally, the target network $Q'$ is updated with the weights of the current action-value function $Q$ every $C$ episodes to stabilize learning.

## V. Evaluation

### A. Cooperation between Satellite and Ground

We employ UERANSIM to simulate the behavior of UE and gNBs [39]. Since UERANSIM lacks support for Xn-based handover, we develop the Xn-based handover function. OpenAirInterface [40] is utilized and modified as RCPF and TCN. The VMs running RCPF and TCN are equipped with Intel(R) Core(TM)2 Duo CPU T7700 @ 2.40GHz, with 4GB and 32GB of memory, respectively. To simulate the operation of RCPF under limited on-board resources, we use the cpulimit tool to restrict the maximum CPU usage of RCPF to 20%.

We consider four common UE-initiated procedures: Xn-based handover, deregistration, PDU session release, and initial registration, which includes PDU session establishment. Table I details the initiation and termination signaling for these procedures. PCT is defined as the duration from the initial request received by the network interface to the final reply issued by the network interface. To assess the impact of satellite-ground collaboration, the signaling associated with the Xn-based handover is processed on the RCPF, while the signaling for the remaining three procedures is processed on the TCN. The experiment involves two gNBs deployed on separate VMs. Initially, a substantial number of UE complete registration and PDU session establishment, laying the groundwork for subsequent procedures. Thereafter, a subset of UE starts the Xn-based handover procedure, while others start deregistration and PDU session release. New UE then initiates registration procedures.

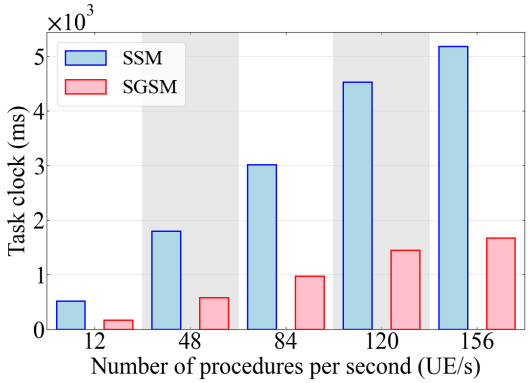


Fig. 6. Average task clock of the RCPF w.r.t. the number of procedures per second.

The time interval between procedures is the inverse of the number of procedures per second. However, due to interactions in Radio Resource Control (RRC) and Radio Link Simulation (RLS) between UE and gNBs, the time interval from trigger by UE to gNB sending signaling varies for each UE. Consequently, the signaling arrival interval at the RCPF can not strictly adhere to predefined intervals. The *Nagle* algorithm in SCTP is disabled to avoid bundling multiple data chunks and delay signaling transmission. To ensure precise measurement of PCT, packets are captured on the network interface of the RCPF using Wireshark tools rather than on the UE. Because the request and response signaling queue in the gNB caused significant fluctuations in PCT. Consequently, it can not adequately reflect the accurate PCT, making comparisons between different methods unreliable.

*1) Number of Procedures Per Second:* First, we compare the CPU usage and PCT relative to the number of procedures per second. Various concurrencies are considered, with values [12, 48, 84, 120, 156], and each scenario is run for 5 seconds. Xn-based handovers constitute 50% of the total procedures, with the remaining three types each accounting for 16.7%. Five experiments are conducted for each scenario, and the results are subsequently aggregated.

The *Perf* tool is used to collect the task clock which represents the duration in which the RCPF is occupying the CPU, as depicted in Fig. 6. Notably, SGSM consistently outperforms Single Satellite Method (SSM) across all concurrency, achieving substantial time savings of approximately 67% (67.0%, 67.7%, 67.5%, 67.9%, and 67.6%, respectively). In SGSM, signaling related to Xn-based handover and signaling sent

TABLE I
Initiation and Termination Signaling for Four Procedures

| **Procedure Type** | **Initiation Signaling** | **Termination Signaling** |
|---|---|---|
| Xn-based Handover | PathSwitchRequest | PathSwitchRequestAcknowledge |
| Registration | InitialUEMessage | PDUSessionResourceSetupRequest |
| Deregistration | DeregistrationRequest | DeregistrationAccept |
| PDU Session Release | PDUSessionReleaseRequest | PDUSessionReleaseCommandAccept |

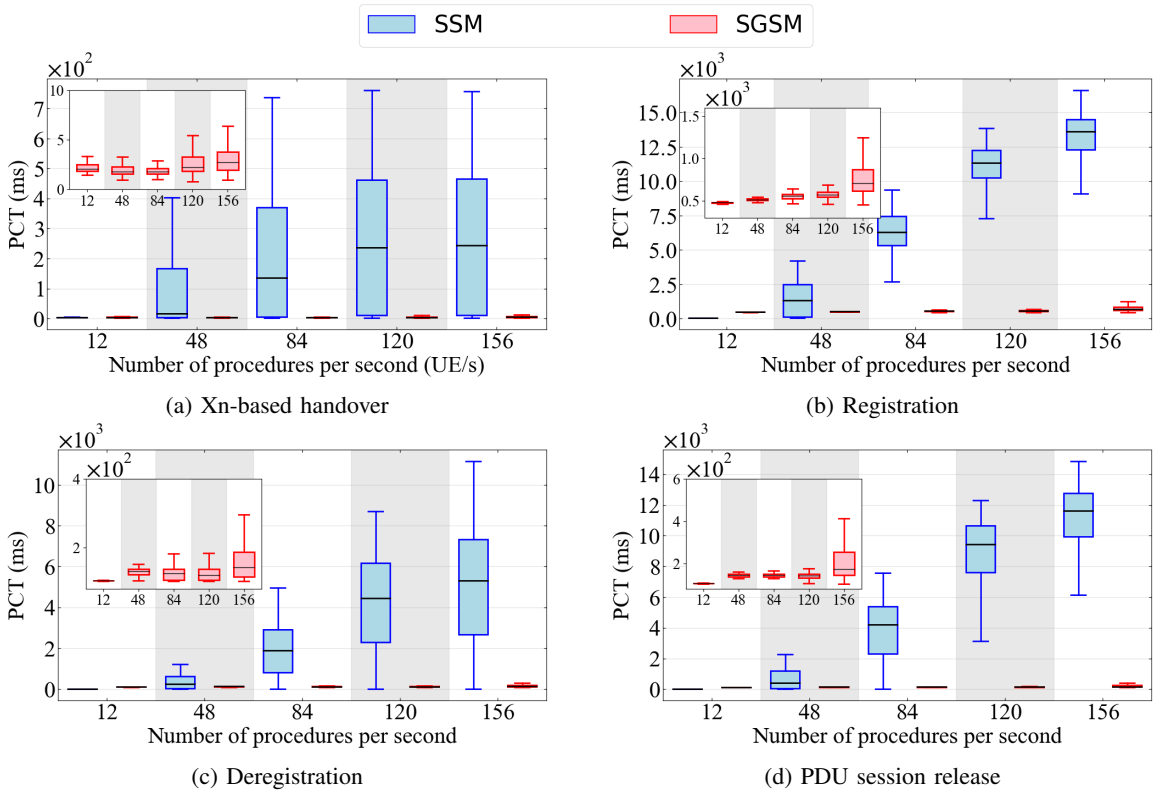


(a) Xn-based handover

(b) Registration

(c) Deregistration

(d) PDU session release

Fig. 7. Procedure completion time w.r.t. the number of procedures per second.

by gNB to CN without requiring a response from CN are processed on-board, while other signaling is forwarded to TCN for processing. In the SSM, which serves as a benchmark, the on-board RCPF solely processes all signaling without distinguishing between time-tolerant and time-sensitive types. SSM does not involve synchronization of UE context with the ground. Reducing the task clock is a crucial advantage for satellites to decrease energy consumption significantly. Additionally, the task clock of SSM grows more rapidly, indicating it sooner exhausts CPU resources. At maximum CPU capacity, the number of signaling processed per second by SSM significantly lags behind SGSM. This difference is attributed to the SGSM forwards signaling to TCN for processing, thus conserving on-board CPU resources.

Fig. 7 illustrates the PCT for the four procedures. In all boxplots, outliers are omitted from the visuals while still being considered in mean value calculations. Both methods display excellent PCT at a concurrency of 12 for Xn-based handover procedures, as shown in Fig. 7 (a). The median PCT for SGSM and SSM are 4.5 ms and 4.4 ms, respectively. Because there is less signaling at this time, and RCPF can process them quickly without causing signaling queuing. However, as concurrency escalates to 48, PCT for SSM experiences a noticeable increase, with the average PCT surging to 101.7 ms. Subsequently, at a concurrency of 84, the average PCT exceeded 200 ms, reaching 205.7 ms, which may cause declined data-plane performance. At a concurrency of 156, over half of the procedures surpassed 243.4 ms. In the small inset at the top-left corner of Fig. 7 (a), the PCT for SGSM exhibited an upward trend but remained at relatively low values. When the concurrency is 156, the average PCT is 6.7 ms, representing a substantial 97.5% reduction compared to SSM's PCT of 266.4 ms. This advantage stems from the RCPF forwarding other signaling to the TCN for processing, with forwarding time notably shorter than processing time. Therefore, the Xn-based handover processing does not need to wait for RCPF to process the other three types of signaling.

SGSM's performance at a concurrency of 12 is inferior to

SSM's for registration (Fig. 7 (b)), deregistration Fig. (7 (c)), and PDU session release procedures (Fig. 7 (d)). Because the additional transmission time between the RCPF and TCN is longer than the RCPF's queuing time. Compared to SSM, the average PCT for registration, deregistration, and PDU session release in SGSM are approximately 425.9 ms, 109.4 ms, and 101.9 ms, respectively. These procedures undergo 4, 1, and 1 Round-Trip Time (RTT) between RCPF and TCN from initiation to completion, respectively. The RTT between the RCPF and TCN is 100 ms in this scenario. However, in absolute terms, the maximum PCT for all three procedures remains below 871 ms, 495 ms, and 166 ms, which are acceptable. As concurrency increases, queuing time becomes a more dominant factor, surpassing the time required for transmission to the TCN. Simultaneously, SSM struggles to handle massive Xn-based handover signaling, leading to delayed processing of the three procedures. When concurrency reached 156, the average PCT for SSM soar to several seconds and, in some cases, even surpassed ten seconds. Although these three procedures are not time-sensitive, such prolonged duration can result in signaling timer expiration, causing UE to perceive signaling failure and initiate the procedure anew.

The RTT value is dynamic due to satellite movement, but our comparison focuses on the relationship between PCT and RTT. Experiments indicate that the primary factors affecting PCT are the number of interactions with the TCN and the RTT value. When the access satellite of the UE and the TCN are on opposite sides of the Earth, the propagation distance is about half an orbit, resulting in an RTT of approximately 158 ms. Although a larger RTT leads to longer PCT, the PCT of three time-tolerant procedures in SGSM remains below 1063 ms, 543 ms, and 214 ms, which are also acceptable.

*2) Percentage of Xn-based handover:* We modified the percentage of the Xn-based handover, and compared the CPU task clock for SSM and SGSM, as depicted in Fig. 8. In SSM, increasing the percentage results in a decrease in the task clock, whereas the SGSM method exhibits the opposite trend. As the percentage rises, the other three procedures utilize fewer CPU resources, causing the performance of the two methods to converge. As the percentage increases, the amount of signaling processed on-board increases, resulting in a higher consumption of computing resources in the SGSM. When the percentage reaches 100%, the task clock of both methods becomes similar, about 1462 ms, as all processing occurs on the RCPF. Registration, deregistration, and PDU session release signaling contain the NAS PDU, whose encryption and decryption lead to higher CPU resource utilization. At a 25% percentage, the task clock for Xn-based handover is only 365.5 ms, accounting for 7.98% (365.5/4580) of the total clocks. However, for SGSM, this percentage rises to 40.8% (365.5/896). Calculations reveal that twelve Xn-based handovers consume approximately 146.2 ms, while four registrations, four deregistrations, and four PDU session releases consume approximately 562 ms. However, forwarding four registrations, four deregistrations, and four PDU session releases to the TCN consumes as little as 70.7 ms. Compared to on-board processing, forwarding signaling to the TCN results in substantial task clock savings of up to 87.4%.

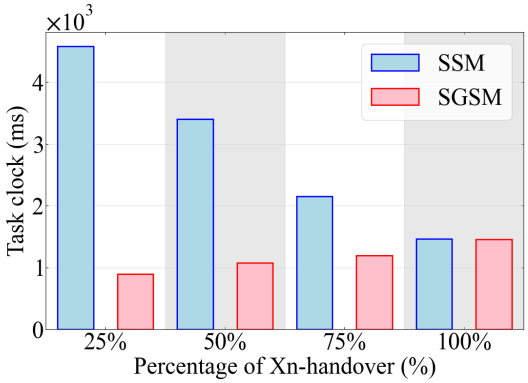


Fig. 8. Average task clock of the RCPF w.r.t. the percentage of Xn-based handover.

In Fig. 9, we present the Cumulative Distribution Functions (CDFs) of PCT for the four procedures in relation to the percentage of Xn-based handovers. In Fig. 9 (a), it is evident that percentage variation exerts a minimal impact on SSM (or SGSM). However, in all three percentage scenarios, SGSM consistently demonstrates superior PCT exceeding 60% compared to SSM. At a 25% percentage, the mean PCT of Xn-based handovers in SSM is 226.1 ms, attributed to the lack of differentiation between time-sensitive and time-tolerant signaling. As the percentage increases to 75%, the mean PCT remains still as high as 173.1 ms. In contrast, the maximum PCT in SGSM does not exceed 15.67 ms.

For the other three procedures, SSM performs poorly at a 25% percentage. The mean PCT for registration (see Fig. 9 (b)) exceeds 12 s, and for deregistration (see Fig. 9 (c)) and PDU session release (see Fig. 9 (d)), it surpasses 4 s and 9 s, respectively, rendering these values intolerable. In SGSM, the mean PCT for these three procedures is reduced to 1065.9 ms, 236.1 ms, and 358.1 ms, respectively. This discrepancy arises because, in SSM, all signaling is queued within the satellite. Conversely, in SGSM, some signaling is queued within the satellite while some is queued on the ground, thereby reducing queuing time. As the percentage increases, the average PCT for registration, deregistration, and PDU session release decreases. At a 75% percentage, the mean PCT for the three procedures in SSM decreases to 3063.9 ms, 934.2 ms, and 1757.4 ms. Fewer messages containing NAS fields expedite signaling processing. Notably, the PCT for the three procedures in SGSM only account for 17%, 12%, and 8% of those in SSM, due to the absence of Xn-based handover signaling in the TCN queue. Frequent handovers between satellites generate a substantial amount of handover signaling. Regardless of the percentage, SGSM's performance is markedly superior to that of SSM.

In SSM, a few PCT are lower than those in SGSM, primarily because signaling is generated for only 5 seconds. As time progresses, a large number of signaling are processed, and the queue becomes not congested, resulting in lower PCT in SSM. However, for SGSM, the transmission time to the TCN increases the PCT, which causes it to exceed SSM.

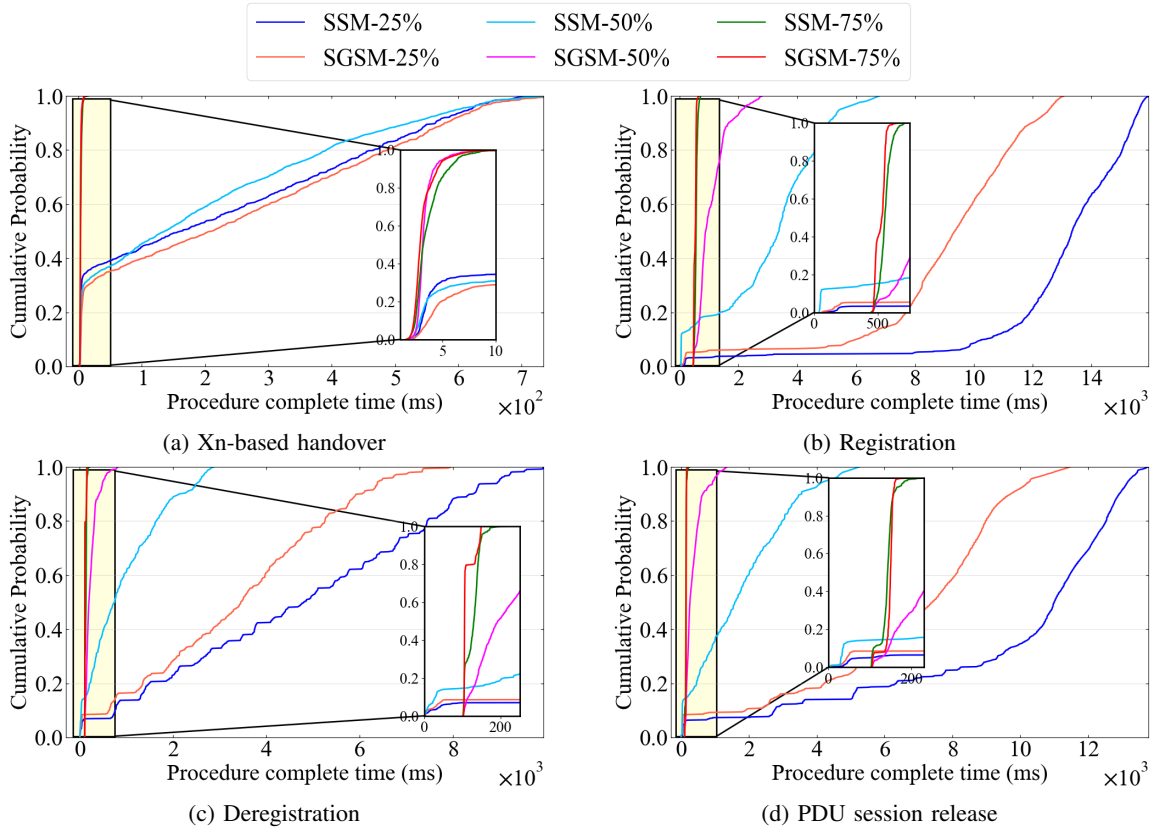


(a) Xn-based handover

(b) Registration

(c) Deregistration

(d) PDU session release

Fig. 9. Procedure completion time w.r.t. percentage of Xn-based handover for all the considered control plane procedures.

### *B. RCPF Migration Procedure*

We compared two methods of transmitting UE context: compressed and uncompressed. The experiment used UE context from the database generated by the stateless AMF to supplant the RCPF. The amount of transferred data with respect to the number of UE is depicted in Fig. 10. The maximum number of UE is 3000. The compression algorithm is Zstandard. In the absence of compression, the total transferred data equates to the product of the number of UE and the size of one UE context. In the compressed scenario, a batch of UE context is extracted from the database and subjected to compression. Experimental results demonstrate that the compression approach significantly reduces the amount of transferred data. The compressed data size is approximately 3% of the uncompressed volume. This reduction can be attributed to the presence of numerous identical fields in the UE context, such as Mobile Country Code (MCC), Mobile Network Code (MNC), Data Network Name (DNN), SMF information, gNB information, among others.

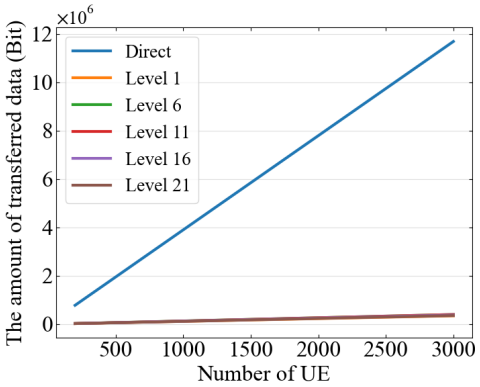


Fig. 10. The amount of transferred data w.r.t the number of UE.

For different compression levels, the size of the compressed data is very similar. However, as depicted in Fig. 11, a lower compression level takes shorter compression and decompression time and occupies fewer task clocks which indicates lower CPU consumption. Both compression and decompression time and task clock exhibit exponential growth with increasing compression levels. The compression and decompression time for level 1 is approximately 2% of the highest level. It is advisable to opt for a lower compression level due to the high degree of data pattern repetition.

We compared the time spent on UE context migration between the compressed transmission scheme and the direct transmission scheme. In the experiments, the uncompressed size of a single UE context is 3895 bytes. When the compression level is set to 1, the compression and decompression time for varying numbers of UE is illustrated in Fig. 12. As the number of UE increases, the compression and decompression time increases linearly. Based on the experiment data, the regression model predicting the compression and decompression

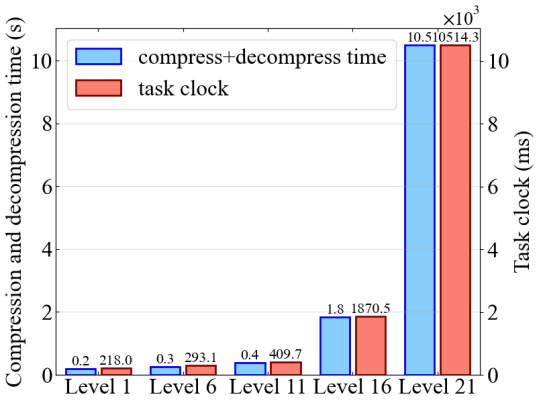


Fig. 11. Compression and decompression time and task clock w.r.t compression level.

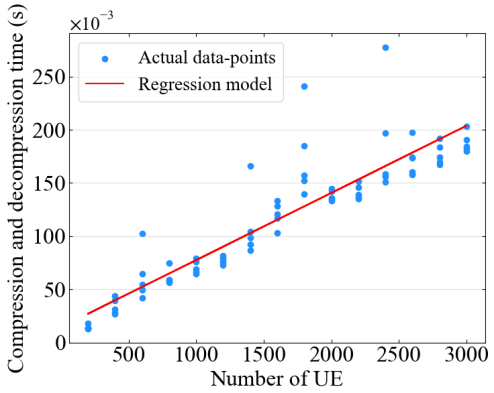


Fig. 12. Regression plot as the number of UE varies, for compression level 1.

time $\phi$ is as follows:

$$\phi = 0.014 + 6.311 \times 10^{-5} \times ue\_num \tag{11}$$

Assuming a bandwidth of 1 Gbps, the direct transmission time can be approximated as $3.895 \times 8 \times 10^{-6} \times ue\_num$ seconds. The amount of transferred data is reduced to 3% of the original amount. The ratio between transmission time with compression and transmission time without compression is:

$$\frac{\phi + 0.03 \times 3.895 \times 8 \times 10^{-6} \times ue\_num}{3.895 \times 8 \times 10^{-6} \times ue\_num} \approx 2.05 \tag{12}$$

Hence, although the cost of the compression method doubles the transmission time, a 97% reduction in transmitted data volume is achieved.

### C. Dynamic Placement of Control Plane

In this experiment, we evaluate the performance of our migration algorithm. We adopt the OneWeb polar constellation [41], comprising 12 orbital planes with 54 satellites in each plane. The period $T$ is 1000 minutes, and the time interval is 20 seconds. The region served by a RCPF ranges in longitude from 93.6°E to 126.8°E, and in latitude from 18°N to 54°N. Different computational resources are allocated to each satellite. We obtain satellite positions at each time slot using

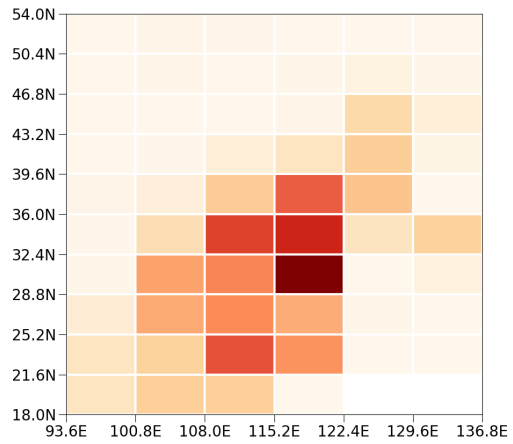


Fig. 13. Distribution of terrestrial UE.

the System Tool Kit (STK) [42], following the rules described in [43]. The population data for each zone is sourced from LandScan Global Population Data [44], as depicted in Fig. 13.

While various strategies exist for S-UPF migration, the deployment algorithm for the S-UPF is beyond the scope of this paper. To maintain generality, we implement a random S-UPF migration strategy. Specifically, when an S-UPF exits the assigned region, it is randomly migrated to another satellite. Furthermore, the new S-UPF location must differ from both the previous S-UPFs and the RCPF positions.

For comparison, we consider the following service deployment methods as benchmarks:

1) **Max Dur**: Migration is initiated only when the RCPF leaves the designated service region, and the target satellite is selected based on the longest duration within the region.
2) **Max CPU**: The RCPF is deployed on the satellite with the highest available computing resources at each time slot. It will be promptly migrated to another satellite whose available resources are richer.
3) **OPtimal**: At each time slot, the RCPF is deployed to the satellite that minimizes the average PCT of Xn-based handover within the service region.

At the initial time slot, the RCPF deployment position for all methods is the optimal position except Max CPU.

Initially, we compare the average PCT of each zone within time $T$ under different methodologies, as depicted in Fig. 14 and Fig. 15. It is evident that Max CPU exhibits the poorest performance, primarily due to the placement of the RCPF at the locations with the highest available computing resources, thereby disregarding the impact of propagation delay. Moreover, satellites with the highest available computing resources also imply fewer UE, rendering the RCPF more likely to be located at the edge of the service region. This increases the propagation time for a substantial number of UE (e.g., as shown in the middle part of Fig. 13), causing significant

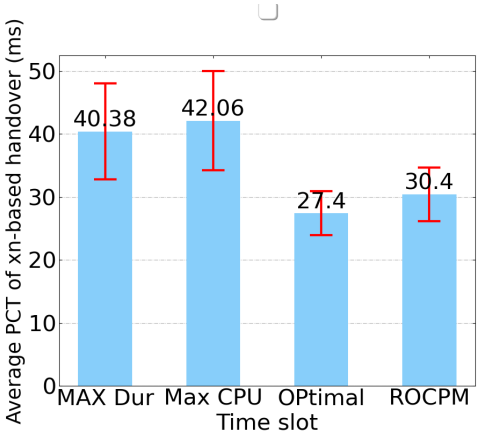


Fig. 14. The average PCT and variance of Xn-based handover within time $T$ under different deployment methods.

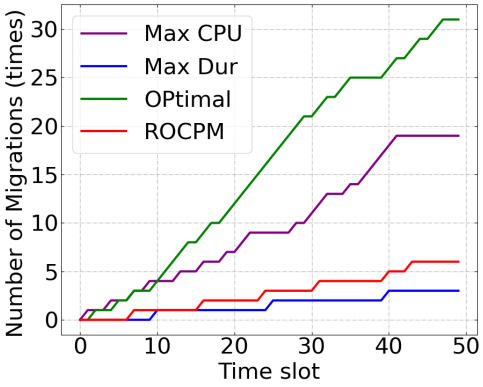


Fig. 16. Number of RCPF migrations over time slots for various deployment methods. The upward trend of the curve signifies the migration of services from one satellite to another.

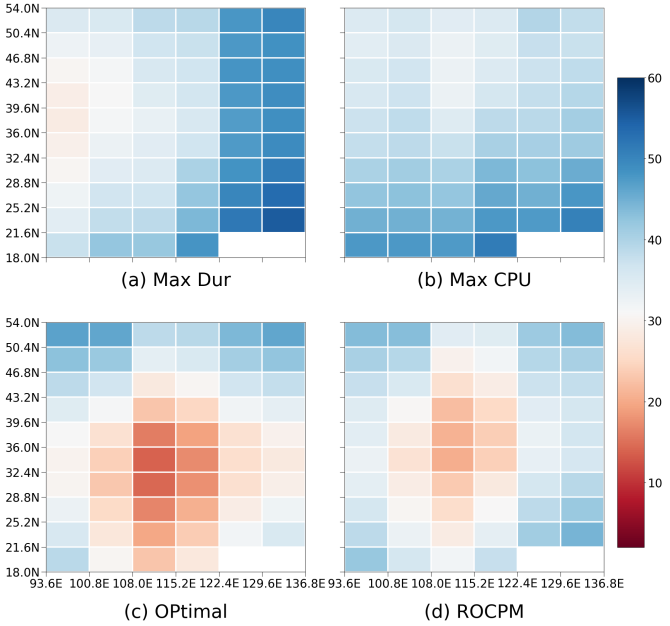


Fig. 15. The average PCT of Xn-based handover in each zone within time $T$ under different deployment methods.

fluctuations in the average PCT. Due to the lower frequency of service migration in Max Dur, it results in a pronounced variance in PCT across zones. Both OPtimal and proposed ROCPM exhibit lower fluctuations compared to Max Dur and Max CPU. For OPtimal, the average PCT in the RCPF service region over time $T$ is 27.4 ms, representing the lowest among all methodologies. This can be attributed to the optimal placement of the RCPF at each time slot. However, while ROCPM is slightly inferior to the OPtimal, its performance remains comparable. The average PCT is 30.4 ms, representing only a marginal increase of approximately 11% compared to OPtimal.

Furthermore, the OPtimal and ROCPM provide different zones with different service quality. Both OPtimal and ROCPM offer superior services for the central hotspot zones. This strategy benefits network providers by enabling them to deliver high-quality services to numerous UE with minimal resource expenditure, thereby boosting their profits. The zone with the lowest PCT is not the one with the most UE, as placing the NF on the satellite serving this zone would significantly increase signaling processing time. Conversely, Max Dur and Max CPU do not take the distribution of UE into consideration.

Due to the additional costs incurred by service migration, we investigate the number of RCPF migrations under different deployment methods, as illustrated in Fig. 16. It is evident that Max Dur exhibits the fewest migrations, which is attributed to its trigger mechanism. As anticipated, both Max CPU and OPtimal methods demonstrate a higher frequency of migrations, with 24 and 31, respectively. In both methods, the RCPF migrates as soon as a better deployment location is found. Conversely, ROCPM achieves comparable performance with only 6 migrations, representing 25% of OPtimal's migrations. Through training, ROCPM effectively migrates by not solely relying on the current state to determine actions but also considering the impact of current actions on the future. Consequently, it optimizes behavior at each time slot, and seeks better migration strategies to minimize the PCT of the Xn-based handover. Compared to the Max Dur, ROCPM performs three extra migrations, leading to a 24.8% reduction in average time. In comparison, the OPtimal method requires 28 additional migrations, only resulting in a 32.2% reduction.

When the traffic density is high, the RCPF coverage region becomes smaller, leading to frequent migrations. But high traffic density often indicates urban areas with TCN. In such areas, the accessing satellite of the UE may only need few hops to reach a nearby TCN. In these situations, there is no need to place the RCPF on the satellite, as the latency between the UE and the TCN is relatively low. Our approach is especially advantageous in remote areas, where the considerable distance to the TCN leads to significant transmission delays. Different deployment strategies should be applied based on the charac-

teristics of various regions. The proposed deployment strategy of mobile networks on satellite networks can collaborate with terrestrial deployment strategies to achieve superior global coverage.

## VI. CONCLUSION

In this paper, our goal was to efficiently integrate terrestrial mobile core networks with LEO satellite networks, thereby enhancing signaling processing performance for UE accessing via satellites. First, to reduce on-board queuing time, we introduced RCPF to redesign the control plane network functions. We proposed SGSM, categorizing signaling into two types: time-sensitive signaling processed on-board and time-tolerant signaling processed on the ground. SGSM leverages terrestrial resources to facilitate on-board processing using the designed UE context synchronization mechanism. Second, to address the increased propagation time due to satellite movement, we designed a migration procedure for RCPF to decrease the amount of transferred data during migration. Additionally, we proposed a migration algorithm considering the distribution of UE and S-UPFs to further optimize the migration strategy. Experiments demonstrated that our proposed satellite-terrestrial integrated core network architecture exhibits superior performance in terms of on-board signaling processing.

## REFERENCES


[1] M. Graydon and L. Parks, "'connecting the unconnected': a critical assessment of us satellite internet services," *Media, Culture & Society*, vol. 42, no. 2, pp. 260–276, 2020.

[2] X. Zhu and C. Jiang, "Integrated satellite-terrestrial networks toward 6g: Architectures, applications, and challenges," *IEEE Internet of Things Journal*, vol. 9, no. 1, pp. 437–461, 2022.

[3] T. Ma, B. Qian, X. Qin, X. Liu, H. Zhou, and L. Zhao, "Satellite-terrestrial integrated 6g: An ultra-dense leo networking management architecture," *IEEE Wireless Communications*, pp. 1–8, 2022.

[4] "SPACEX SENDS FIRST TEXT MESSAGES VIA ITS NEWLY LAUNCHED DIRECT TOCELL SATELLITES," 2024. [Online]. Available: https://api.starlink.com/public-files/DIRECT_TO_CELL_FIRST_TEXT_UPDATE.pdf

[5] *Solutions for NR to support Non-Terrestrial Networks (NTN)*, 3GPP Standard (TR) 38.821 V16.1.0, May. 2021. [Online]. Available: https://www.3gpp.org/ftp/Specs/archive/38_series/38.821

[6] X. Li, Q. Cui, Q. Xue, W. Ni, J. Guo, and X. Tao, "A new batch access scheme with global qos optimization for satellite-terrestrial networks," in *GLOBECOM 2022 - 2022 IEEE Global Communications Conference*, 2022, pp. 3929–3934.

[7] Y. Liu, L. Wang, Z. Lu, K. Du, and G. Shou, "A stateless design of satellite-terrestrial integrated core network and its deployment strategy," *IEEE Transactions on Network and Service Management*, pp. 1–1, 2023.

[8] J. Kim, J. Lee, H. Ko, T. Kim, and S. Pack, "Space mobile networks: Satellite as core and access networks for b5g," *IEEE Communications Magazine*, vol. 60, no. 4, pp. 58–64, 2022.

[9] H. Cui, J. Zhang, Y. Geng, Z. Xiao, T. Sun, N. Zhang, J. Liu, Q. Wu, and X. Cao, "Space-air-ground integrated network (sagin) for 6g: Requirements, architecture and challenges," *China Communications*, vol. 19, no. 2, pp. 90–108, 2022.

[10] S. Wang and Q. Li, "Satellite computing: Vision and challenges," *IEEE Internet of Things Journal*, pp. 1–1, 2023.

[11] R. Xing, X. Ma, A. Zhou, S. Dustdar, and S. Wang, "From earth to space: A first deployment of 5g core network on satellite," *China Communications*, vol. 20, no. 4, pp. 315–325, 2023.

[12] Z. Han, C. Xu, K. Liu, L. Yu, G. Zhao, and S. Yu, "A novel mobile core network architecture for satellite-terrestrial integrated network," in *2021 IEEE Global Communications Conference (GLOBECOM)*, 2021, pp. 01–06.

[13] Y. Sun, M. Peng, S. Zhang, G. Lin, and P. Zhang, "Integrated satellite-terrestrial networks: Architectures, key techniques, and experimental progress," *IEEE Network*, vol. 36, no. 6, pp. 191–198, 2022.

[14] Y. Liu, L. Wang, Z. Lu, and G. Shou, "A qos guaranteed efficient integration of upf and leo satellite networks," *IEEE Transactions on Network and Service Management*, pp. 1–1, 2024.

[15] S. Ji, M. Sheng, D. Zhou, W. Bai, Q. Cao, and J. Li, "Flexible and distributed mobility management for integrated terrestrial-satellite networks: Challenges, architectures, and approaches," *IEEE Network*, vol. 35, no. 4, pp. 73–81, 2021.

[16] C. Li, Y. Zhang, R. Xie, X. Hao, and T. Huang, "Integrating edge computing into low earth orbit satellite networks: Architecture and prototype," *IEEE Access*, vol. 9, pp. 39 126–39 137, 2021.

[17] C. Han, A. Liu, L. Huo, H. Wang, and X. Liang, "A prediction-based resource matching scheme for rentable leo satellite communication network," *IEEE Communications Letters*, vol. 24, no. 2, pp. 414–417, 2020.

[18] G. Cui, P. Duan, L. Xu, and W. Wang, "Latency optimization for hybrid geo–leo satellite-assisted iot networks," *IEEE Internet of Things Journal*, vol. 10, no. 7, pp. 6286–6297, 2023.

[19] C. Li, Y. Zhang, X. Hao, and T. Huang, "Jointly optimized request dispatching and service placement for mec in leo network," *China Communications*, vol. 17, no. 8, pp. 199–208, 2020.

[20] H. Zhang, R. Liu, A. Kaushik, and X. Gao, "Satellite edge computing with collaborative computation offloading: An intelligent deep deterministic policy gradient approach," *IEEE Internet of Things Journal*, vol. 10, no. 10, pp. 9092–9107, 2023.

[21] H. Han, H. Wang, and S. Cao, "Space edge cloud enabling service migration for on-orbit service," in *2020 12th International Conference on Communication Software and Networks (ICCSN)*, 2020, pp. 233–239.

[22] A. Papa, T. de Cola, P. Vizarreta, M. He, C. Mas-Machuca, and W. Kellerer, "Design and evaluation of reconfigurable sdn leo constellations," *IEEE Transactions on Network and Service Management*, vol. 17, no. 3, pp. 1432–1445, 2020.

[23] Z. Li, H. Zhang, C. Liu, X. Li, H. Ji, and V. C. M. Leung, "Online service deployment on mega-leo satellite constellations for end-to-end delay optimization," *IEEE Transactions on Network Science and Engineering*, vol. 11, no. 1, pp. 1214–1226, 2024.

[24] A. Mohammadkhan, K. K. Ramakrishnan, and V. A. Jain, "Cleang—improving the architecture and protocols for future cellular networks with nfv," *IEEE/ACM Transactions on Networking*, vol. 28, no. 6, pp. 2559–2572, 2020.

[25] V. Jain, H.-T. Chu, S. Qi, C.-A. Lee, H.-C. Chang, C.-Y. Hsieh, K. K. Ramakrishnan, and J.-C. Chen, "L25gc: A low latency 5g core network based on high-performance nfv platforms," in *Proceedings of the ACM SIGCOMM 2022 Conference*, ser. SIGCOMM '22. New York, NY, USA: Association for Computing Machinery, 2022, p. 143–157.

[26] E. Goshi, R. Stahl, H. Harkous, M. He, R. Pries, and W. Kellerer, "Pp5gs—an efficient procedure-based and stateless architecture for next-generation core networks," *IEEE Transactions on Network and Service Management*, vol. 20, no. 3, pp. 3318–3333, 2023.

[27] J. Choi, N. Sharma, S. S. Gantha, V. Mandawaria, J. Cha, D. Kim, J. Jung, J. Lee, and S. Choi, "Ran-cn converged control-plane for 6g cellular networks," in *GLOBECOM 2022 - 2022 IEEE Global Communications Conference*, 2022, pp. 1253–1258.

[28] J. Larrea, A. E. Ferguson, and M. K. Marina, "Corekube: An efficient, autoscaling and resilient mobile core system," in *Proceedings of the 29th Annual International Conference on Mobile Computing and Networking*, ser. ACM MobiCom '23. New York, NY, USA: Association for Computing Machinery, 2023.

[29] K. Du, L. Wang, X. Wen, Y. Liu, H. Niu, and S. Huang, "Ml-sld: A message-level stateless design for cloud-native 5g core network," *Digital Communications and Networks*, vol. 9, no. 3, pp. 743–756, 2023. [Online]. Available: https://www.sciencedirect.com/science/article/pii/S2352864822000815

[30] Y. Sun, M. Peng, S. Zhang, G. Lin, and P. Zhang, "Integrated satellite-terrestrial networks: Architectures, key techniques, and experimental progress," *IEEE Network*, vol. 36, no. 6, pp. 191–198, 2022.

[31] Z. Yan, T. d. Cola, K. Zhao, W. Li, S. Du, and H. Yang, "Exploiting edge computing in internet of space things networks: Dynamic and static server placement," in *2021 IEEE 94th Vehicular Technology Conference (VTC2021-Fall)*, 2021, pp. 1–6.

[32] Y. Li, H. Li, W. Liu, L. Liu, Y. Chen, J. Wu, Q. Wu, J. Liu, and Z. Lai, "A case for stateless mobile core network functions in space," in *Proceedings of the ACM SIGCOMM 2022 Conference*, ser. SIGCOMM '22. New York, NY, USA: Association for Computing Machinery, 2022, p. 298–313.

[33] *System Architecture for the 5G System*, 3GPP Standard (TS) 23.501, Dec. 2019. [Online]. Available: https://www.3gpp.org/ftp/Specs/archive/23_series/23.501/
[34] I. Leyva-Mayorga, B. Soret, and P. Popovski, "Inter-plane inter-satellite connectivity in dense leo constellations," *IEEE Transactions on Wireless Communications*, vol. 20, no. 6, pp. 3430–3443, 2021.
[35] Y. Zhang, Q. Wu, Z. Lai, and H. Li, "Enabling low-latency-capable satellite-ground topology for emerging leo satellite networks," in *IEEE INFOCOM 2022 - IEEE Conference on Computer Communications*, 2022, pp. 1329–1338.
[36] Q. Li, S. Wang, X. Ma, Q. Sun, H. Wang, S. Cao, and F. Yang, "Service coverage for satellite edge computing," *IEEE Internet of Things Journal*, vol. 9, no. 1, pp. 695–705, 2022.
[37] S. Pramanik, A. Ksentini, and C. Fabiana Chiasserini, "Characterizing the computational and memory requirements of virtual rans," in *2022 17th Wireless On-Demand Network Systems and Services Conference (WONS)*, 2022, pp. 1–8.
[38] P. Chardaire, A. Sutter, and M.-C. Costa, "Solving the dynamic facility location problem," *Networks*, vol. 28, no. 2, pp. 117–124, 1996. [Online]. Available: https://onlinelibrary.wiley.com/doi/abs/10.1002/%28SICI%291097-0037%28199609%2928%3A2%3C117%3A%3AAID-NET5%3E3.0.CO%3B2-H
[39] A. Güngör, "aligungr/UERANSIM," https://github.com/aligungr/UERANSIM, 2023, accessed: 2024-01-29.
[40] cn5g · GitLab. [Online]. Available: https://gitlab.eurecom.fr/oai/cn5g
[41] Our network. [Online]. Available: http://oneweb.net/our-network
[42] "Systems Tool Kit (STK)," 2021. [Online]. Available: https://www.agi.com/products/stk
[43] Astrome, "The art of satellite constellation design: What you need to know," 2015. [Online]. Available: https://astrome.net/blogs/the-art-of-satellite-constellation-design-what-you-need-to-know/
[44] LandScan Dataset, "Landscan 2019," 2019. [Online]. Available: https://landscan.ornl.gov/download/

**Yu Liu** received his B.S. degree from Communication University of China in 2020. He is currently working toward the Ph.d. degree in communications engineering with the Beijing University of Posts and Telecommunications, China. His current research interests include network architecture, network function virtualization, mobile core network, and IoT network

**Luhan Wang** received the Ph.D. degree from the Beijing University of Posts and Telecommunications (BUPT) in 2017. In 2016, he visited Eurecom as a visiting Ph.D. student. In 2017, he joined the School of Information and Communication Engineering, BUPT, as an Assistant Professor. He also works as a researcher and project manager in Joint BUPT Eurecom Open5G Lab. His research interests include network architecture, network function virtualization, and software-defined networks. He currently leads a team in BUPT which is getting involved in OpenAirInterface 5G CN development.

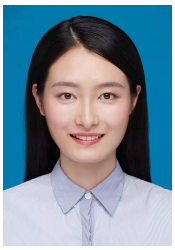

**Ao Liu** received her B.S. degree from University of Science and Technology Beijing in 2020. She is now in pursuit of the Ph.D. degree from Beijing University of Posts and Telecommunications. Her research interests include wireless communication, joint communication and sensing network, and IoT.

**Zhaoming Lu** received the B.S. degree in communication engineering from Zhengzhou University, Zhengzhou, China, in 2007, and trhe Ph.D. degree in information and communication engineering from the Beijing University of Posts and Telecommunications, Beijing, China, in 2012. He is currently an Professor with the School of Information and Communication Engineering, Beijing University of Posts and Telecommunications. His research interests include opensource 5G, network-aided autonomous driving, and WiFi sensing and imaging. He was the General Chair, the TPC Chair, a TPC Member for several international workshops and conferences, and he is on the Editorial Board of two international journals. He was the recipient of the Best Paper Award of IEEE ICEI 2018 and Best Demo of IEEE ISWCS 2016.

**Guochu Shou** is currently a professor at the School of Information and Communication Engineering, Beijing University of Posts and Telecommunications. His research interests include access network and edge computing, fiber and wireless network virtualization, network construction and routing, and mobile Internet and applications.

**Adlen Ksentini** (Senior Member, IEEE) is a professor in the Communication Systems Department of EURECOM. He is leading the Network softwarization group activities related to Network softwarization, 5G/6G, and Edge Computing. Adlen Ksentini's research interests are Network Sofwerization and Network Cloudification, focusing on topics related to network virtualization, Software Defined Networking (SDN), and Edge Computing for 5G and 6G networks. He has been participating to several H2020 and Horizon Europe projects on 5G and beyond, such as 5G!Pagoda, 5GTransformer, 5G!Drones, MonB5G, ImagineB5G, 6GBricks, 6G-Intense, Sunrise-6G and AC3. He is the technical manager of 6G-Intense and AC3, on zero-touch management of 6G resources and applications, and Cloud Edge Continuum, respectively. He is interested in the system and architectural issues but also in algorithm problems related to those topics, using Markov Chains, Optimization algorithms, and Machine Learning (ML). Adlen Ksentini has given several tutorials in IEEE international conferences, IEEE Globecom 2015, IEEEE CCNC 2017/2018/2023, IEEE ICC 2017, IEEE/IFIP IM 2017, IEEE School 2019. Adlen Ksentini is a member of the OAI board of directors, where he is in charge of OAI 5G Core Network and O-RAN management (O1, E2) for OAI RAN activities.